Modal decomposition of flow behind a harmonically oscillating circular cylinder

Sudeep Menon[1], Xingeng Wu[1,2], Anupam Sharma[1*]

[1]Aerospace Engineering, Iowa State University, 537 Bissell Road, Ames, 50011, Iowa, USA.
[2]Now at Midea Group, China.

*Corresponding author(s). E-mail(s): sharma@iastate.edu;
Contributing authors: smenon@iastate.edu; xgwu@iastate.edu;

Abstract

We examine the flow behavior around a transversely oscillating circular cylinder using various dimensionality reduction techniques. Specifically, Fourier analysis, Proper Orthogonal Decomposition (POD), Dynamic Mode Decomposition (DMD), and multi-resolution DMD (mrDMD) are employed. Numerical simulations are performed at a cylinder-diameter-based Reynolds number of 500 for a range of oscillation displacement amplitudes. The flow field exhibits well-documented wake patterns, such as 2S, 2P, and P+S, as well as intermittent transitions between these patterns at varying amplitudes. Dimensionality reduction becomes particularly effective when the force spectrum exhibits a dominant tonal character. Under these circumstances, the selection of the modal decomposition technique has minimal impact—all approaches yield comparable mode shapes for the dominant modes. However, when the flow undergoes intermittent pattern switching (e.g., between 2P and 2S), only mrDMD is able to *automatically* distinguish them as distinct modes. Nonetheless, if the temporal windows over which mode switching occurs are specified a priori, POD, DMD, and DFT are also successful.

Keywords: vortex shedding, DMD, POD, DFT, mRDMD

1 Introduction

Vortex induced vibration (VIV) is a common occurrence and a source of problem in many engineering structures, such as marine risers, power conductors, cables, etc. VIV refers to a finite amplitude oscillatory motion that is setup in a structure due to force excitation by Kármán vortex shedding in its wake. Large amplitudes are observed when the excitation frequency synchronizes with the natural frequency of the structure, a phenomenon known as "lock in". A key parameter affecting VIV is the combined mass-damping parameter ($m^*\zeta$). Variants of this parameter, such as the Scruton number (S_c) and the Skop-Griffin parameter (S_G), have been used to characterize VIV (Vandiver, 2012).

VIV in low mass-damping systems is characteristically different from that in high mass-damping systems. The Griffin plot (normalized amplitude versus reduced velocity) for a low-mass damping system exhibits a "lower" branch in the lock-in region, which is not observed in high mass-damping systems. Other branches – "initial excitation", "upper", and "desynchronization" – are observed in both low and high mass-damping systems (see Fig. 1). The different branches are characterized not only by difference in the amplitude of vibration, but also by spatio-temporal correlations in the wake of the vibrating structure. These correlations are referred to as "modes" in the literature. A few vortex modes that are commonly observed during VIV

include 2S (two single vortices), 2P (pairs of vortices), and P+S (a pair of vortices and a single vortex). These are identified and illustrated on the Griffin plot for VIV of a low mass-damping system in Fig. 1.

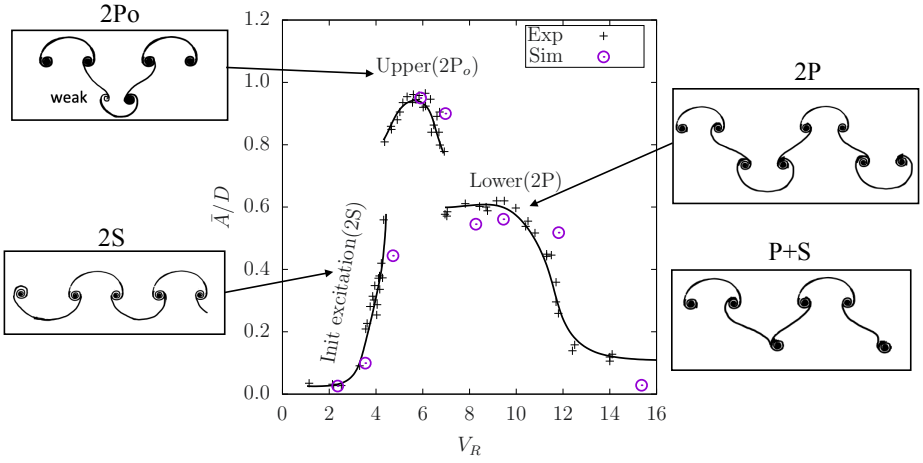

Fig. 1: The different branches observed experimentally and numerically in VIV of a low mass-damping circular cylinder are shown here. The corresponding vortex patterns/modes are identified in brackets in the center panel and illustrated with sketches in the smaller side panels. Experimental data is from Khalak and Williamson (1997) and simulation results are from Wu et al. (2020). $V_R = V_\infty/(f_N D)$ is the reduced velocity, where f_N is the natural frequency, D is the cylinder diameter, and V_∞ is the inflow velocity.

Controlled (prescribed) motion experiments and simulations are widely used to investigate the fundamental phenomena associated with VIV, e.g., Leontini et al. (2006) and Sarpkaya (2004). Through their prescribed-motion experiments, Williamson and Roshko (1988) generated an extensive map of wake/vortex modes for $300 < Re < 500$ (Re is the diameter-based Reynolds number) and observed the 2S, 2P, and P+S wake/vortex modes. Morse and Williamson (2006) demonstrated that fluid forces measured in prescribed motion experiments (transverse, constant-amplitude oscillation of a circular cylinder) agree well with those measured for free vibration, provided the experimental conditions are precisely matched. Morse and Williamson (2009) used their prescribed-motion data to predict VIV; their predictions show excellent agreement with free vibration measurements. We therefore focus on analyzing prescribed-motion simulations with applications to VIV.

Through an extensive experimental campaign involving over 6000 runs, Morse and Williamson (2009) compiled high-resolution contour plots (on a normalized amplitude and reduced frequency plane) of fluid force and the phase angle between force and displacement. They observed remarkable similarity between boundaries separating different fluid-forcing regimes in these plots and the boundaries separating the different wake/vortex modes in the map presented by Williamson and Roshko (1988); Fig. 2 shows their map of fluid force with boundaries delineating the different wake/vortex mode regimes. Some very interesting phenomena involving *hysteresis* (as the reduced velocity is varied) and *intermittency* (mode switching) have been observed through high-resolution digital particle image velocimetry (PIV) measurements by Govardhan and Williamson (2000).

Identification of these modes has primarily been done by visualizing the flow field, e.g., using contours of spanwise vorticity. Given the richness of fundamental flow phenomena that can be revealed through investigating wake/vortex modes and the strong correlation between these modes and the loading (and dynamics in the case of free vibration) on the cylinder, we present detailed modal decomposition of the flow behind an oscillating circular cylinder. Specifically, we aim to answer the following questions in the context of this problem. 1) Is the dynamical system always amenable to dimensional reduction? 2) Which modal decomposition technique is able to best describe the system and under what conditions? and 3) Can intermittent flow patterns be separated into distinct modes?

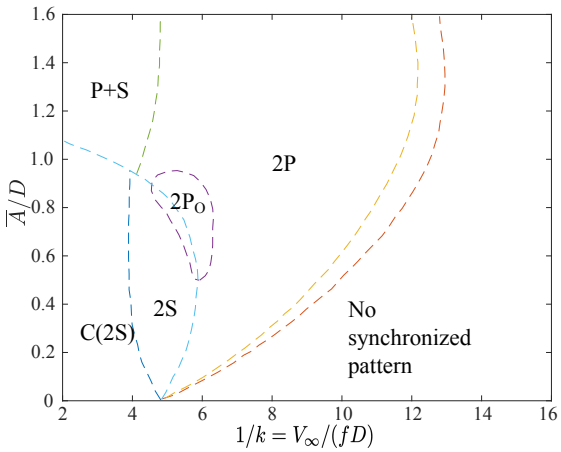

Fig. 2: Map of wake modes; adapted from Morse and Williamson (2009).

2 Methods

2.1 Flow simulation

We perform detached eddy simulations (DES) of flow over a circular cylinder undergoing prescribed transverse oscillatory motion. The flow is assumed to be incompressible, and the governing equations are

$$\frac{\partial \tilde{U}_i}{\partial x_i} = 0 \quad \text{and} \quad \frac{\partial \tilde{U}_i}{\partial t} + \frac{\partial (\tilde{U}_j \tilde{U}_i)}{\partial x_j} = -\frac{1}{\rho}\frac{\partial \tilde{p}}{\partial x_i} + \nu \frac{\partial^2 \tilde{U}_i}{\partial x_j^2} - \frac{\partial \tau_{ij}}{\partial x_j}. \tag{1}$$

The overhead tilde denotes a spatially filtered quantity, $\tau_{ij} = \widetilde{U_i U_j} - \tilde{U}_i \tilde{U}_j = -2\,\nu_{\text{SGS}}\,\tilde{S}$, $\tilde{S} = (\partial \tilde{U}_i/\partial x_j + \partial \tilde{U}_j/\partial x_i)/2$, and ν_{SGS} is the sub-grid scale (eddy) viscosity. A dynamic procedure is used to switch between Reynolds-averaged Navier-Stokes (RANS) and large eddy simulations (LES). The specific hybrid RANS-LES (DES) approach used here has been verified for simulating flow past rigidly and elastically mounted cylinders (see Wu and Sharma, 2020; Wu, 2020; Wu et al., 2020, 2017).

A k-ω turbulence closure model is used; the transport equations for k and ω are

$$\begin{aligned} \frac{Dk}{Dt} &= 2\nu_T |S|^2 - C_\mu k\omega + \partial_j[(\nu + \sigma_k \nu_T)\partial_j k], \\ \frac{D\omega}{Dt} &= 2C_{\omega 1}|S|^2 - C_{\omega 2}\omega^2 + \partial_j[(\nu + \sigma_\omega \nu_T)\partial_j \omega]. \end{aligned} \tag{2}$$

The DES length scale, l_{DES} is defined as

$$l_{\text{DES}} = l_{\text{RANS}} - \max(0,\ l_{\text{RANS}} - l_{\text{LES}}), \tag{3}$$

where $l_{\text{RANS}} = \sqrt{k}/\omega$ and $l_{\text{LES}} = C_s \triangle$ are the RANS and LES length scales respectively; $\triangle = V^{1/3}$ represents the cell size. The switch between the RANS and LES branches is seamless. In regions where the mesh density is high (small $\triangle \rightarrow l_{\text{LES}} < l_{\text{RANS}}$), $l_{\text{DES}} = l_{\text{LES}}$ and the LES model is active with the $k-\omega$ model serving as a sub-grid model ($\nu_{\text{SGS}} = l_{\text{DES}}^2\,\omega = (C_s \triangle)^2\,\omega$). Elsewhere, $l_{\text{DES}} = l_{\text{RANS}}$ and the RANS model is active with the $k-\omega$ model serving as a RANS closure model ($\nu_T = l_{\text{DES}}^2\,\omega = k^2/\omega$).

In the current simulations the cylinder undergoes a prescribed harmonic transverse oscillatory motion at a frequency (f) that corresponds to the Strouhal number, St of the cylinder under static conditions ($St = 0.2$). The non-dimensional frequency $k = fD/V_\infty$, where D is the cylinder diameter and V_∞ is the freestream flow speed. The diameter-based Reynolds number, Re is 500. At this Re, laminar vortex shedding is observed in the wake. While the wake is unstable to 3D perturbations at this Re, the vortex shedding behavior and modes/patterns can be qualitatively captured by two-dimensional simulations. Therefore, while the DES

strategy is adopted, the simulations are two-dimensional. The differences between 2D and 3D are expected to be larger in higher-order (lower-energy) modes.

Figure 3 shows the different vortex modes observed as the scaled displacement amplitude (A/D) is varied between 0.2 and 1.0. Four distinct modes are visually identified in the simulation results: 2S, P+S, 2P/2S, and 2P. These can be seen in the time evolution snapshots in Fig. 4. The label '2P/2S' denotes cases where the solution intermittently switches between the 2P and 2S modes. This intermittent mode switching is evident in Fig. 4 for $A/D = 0.8$. We next describe the first three modal decomposition approaches used in this paper to analyze these simulation results; mrDMD is discussed in a later section.

A/D	Mode(s)	#POD modes to capture 90% energy	99% energy
0.2	2S	-	-
0.25	2S	8	20
0.3	2S	-	-
0.4	P+S	-	-
0.5	P+S	10	26
0.6	P+S	-	-
0.7	2S	-	-
0.75	2S	13	60
0.8	2P/2S	-	-
0.9	2P/2S	41	122
1.0	2P	13	34

(a)

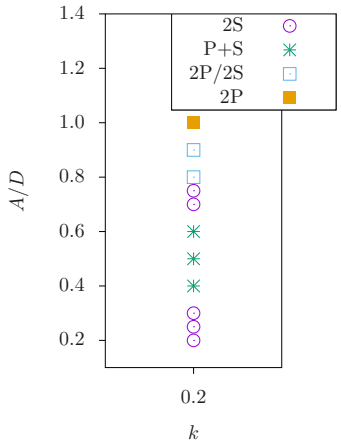

(b)

Fig. 3: Different prescribed harmonic-motion simulations and the observed vortex modes in (a) a tabular form, and (b) a visual representation to show the mode boundaries. The highlighted rows in the table indicate the cases that are analyzed using different modal decomposition techniques. $k = 0.2$ for all cases.

2.2 Modal decomposition

The simulation results are projected onto a uniform 2D rectangular mesh (650×400) in the region $1 \leq x/D \leq 8$ and $-2.5 \leq y/D \leq 2.5$ for modal analysis. We first evaluate the following three approaches for modal decomposition: 1) Fourier analysis, 2) Proper Orthogonal Decomposition (POD), and 3) Dynamic Mode Decomposition (DMD). Fourier analysis is routinely used for spectral analysis of scalar data series, such as lift and displacement spectra. Here we utilize it to decompose the entire wake flow field into Fourier modes, where each mode is associated with a fixed frequency. Fourier transforms are performed over eight cylinder oscillation periods; data are collected after the initial transients have been removed from the simulations. When computing Fourier modes, the results are neither phase-averaged (over multiple cycles) nor spectrally averaged (Welch, 1967) to ensure that the intrinsic flow dynamics is not distorted by such averaging.

Principal Component Analysis, commonly referred to as Proper Orthogonal Decomposition (POD) in fluid mechanics, is a data-driven dimensional reduction technique that identifies correlations in data. POD was first used by Lumley (1967) to analyze the structure of turbulent flows. POD can extract an orthonormal basis (modes) from an ensemble of data, ranking them from highest to lowest variance (energy content) of the system (Berkooz et al., 1993). A popular way to perform POD is by computing the singular value decomposition (SVD) of the data matrix $\mathcal{X} = \mathcal{U}\Sigma\mathcal{V}^*$, where the right singular vectors ($\mathcal{U}$) contain the mode shapes, Σ is a diagonal matrix of the singular values (variance), and $\mathcal{V}$ are the left singular vectors; $\mathcal{U}$ and $\mathcal{V}$ are unitary matrices (for a full SVD). If $\mathcal{X}$ consists of a series of time measurements arranged as column vectors then $\mathcal{U}$ contains spatially correlated modes and $\mathcal{V}$ contains temporal information. The modes (columns of $\mathcal{U}$) are spatially orthogonal but not temporally orthogonal; each mode can have multiple frequencies. Huera-Huarte and Vernet (2010) used POD in combination with Fuzzy Clustering for dimensional reduction and classification of wake patterns behind a flexible cylinder experiencing VIV.

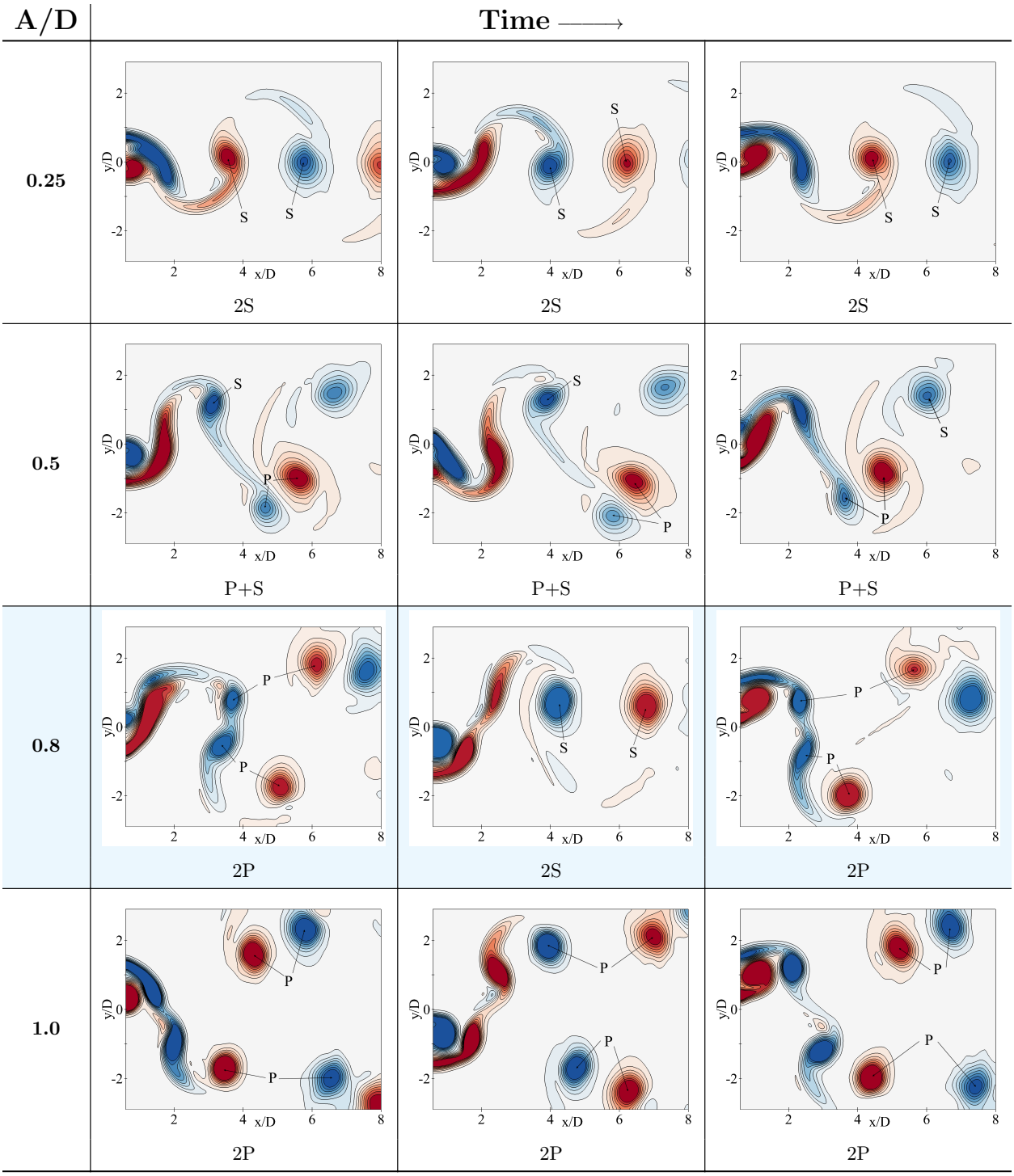

Fig. 4: Time evolution contours of spanwise vorticity showing different wake patterns: 2S for $A/D = 0.25$, P+S for $A/D = 0.5$, 2P/2S for $A/D = 0.8$, and 2P for $A/D = 1.0$. For $A/D = 0.8$ (highlighted row), the pattern switches between 2P and 2S.

Dynamic mode decomposition (DMD) approximates the modes of the Koopman operator, an infinite-dimensional linear operator capable of representing any nonlinear dynamical system. In DMD, the infinite-dimensional Koopman operator is reduced to a finite-dimensional linear model. As such, DMD is a

dimensionality-reduction technique. DMD was introduced by Schmid (2010) and first applied to analyze the dynamics of fluid flow. It has been widely use to study cylinder wake flow, particularly for stationary cases. Tissot et al. (2013) employed DMD to analyze PIV measurements for a static cylinder wake at $Re = 40,000$ and concluded that three pairs of DMD modes are sufficient to represent the original dynamics. Bagheri (2013) conducted a Koopman analysis of the cylinder wake and demonstrated that DMD modes approximate Koopman modes under certain conditions. Kou et al. (2017) used DMD to study the lowest Reynolds number at which VIV occurs. Wang and Liu (2017) performed a DMD analysis of flow over a vibrissa-shaped cylinder undergoing VIV and found that the dominant modes and frequency varied with spanwise location.

DMD is completely data driven and requires no information about the governing equations of the dynamical system. DMD can robustly and reliably decompose complex flow fields into spatio-temporal coherent modes (Kutz et al., 2016). Unlike POD, each DMD mode is only associated with a single frequency and a decay/growth rate, i.e., DMD modes are temporally orthogonal. However, DMD modes do not represent variance (energy content) of the system. For the results presented here, DMD modes are computed using the SVD approach, retaining as many singular vectors as needed to capture 99%, or in some cases 90%, of the energy (variance) in the signal.

As shown later, these modal decomposition techniques do not work well when pattern/mode switching is observed (e.g., $A/D = 0.8$ in Fig. 4). The multiresolution DMD or mrDMD (Kutz et al., 2016) approach for modal decomposition is attempted for such cases. mrDMD integrates the classic DMD algorithm with key concepts from wavelet analysis. This combination enables multiresolution analysis simultaneously in space and time, allowing multi-scale spatiotemporal features to be readily separated. mrDMD is inspired by the observation that slow or low-frequency modes can be separated from fast modes. It commences with the application of DMD on an appropriate collection of snapshots containing all content (both high- and low-frequency) to obtain a full-rank approximation of the dynamics. The slowest modes are removed from this initial pass, and the domain is divided into two halves. DMD is performed on each half of the collection of snapshots. Again, the slowest modes are removed, and the process is repeated until the desired result is achieved

3 Results and discussion

Five of the eleven simulated cases (see highlighted rows in Fig. 3a) are analyzed using the modal decomposition techniques summarized in Section 2.2. The spanwise vorticity ($\Omega_z = \partial_y u - \partial_x v$) field in the wake, evaluated in the ground frame of reference, is used for modal decomposition. Section A discusses the differences that arise if a frame of reference attached to the cylinder is used.

3.1 2S mode, $A/D = 0.25$

Figure 5a plots the power spectral densities (PSDs) of the normal and tangential force coefficients, $C_y = F_y/(q_\infty D)$ and $C_x = F_x/(q_\infty D)$, respectively, for the case where $A/D = 0.25$; $q_\infty = \rho_\infty U_\infty^2/2$ is the dynamic pressure. The spectra show dominant peaks at the Strouhal number ($St \sim k = 0.2$) and its harmonics. Odd harmonics ($k = 0.6, 1.0, \ldots$) are observed in the C_y spectrum, while even harmonics ($k = 0.4, 0.8, \ldots$) are present in the C_x spectrum. This is consistent with the observations for flow over a static cylinder (Wu et al., 2020). The existence of only a handful of dominant peaks in the spectra suggests the feasibility of dimensional reduction. This is evident from the plot of singular values (Fig. 5b) and the table in Fig. 3a, which show that 90% of the signal energy is contained in the first eight singular vectors (POD modes).

Figure 5c plots the DMD eigenvalues (λ), which fall on the unit circle at equispaced angular positions, suggesting that all the modes are harmonic functions with no growth/decay in time. The angular position of λ (measured from the positive x axis in the eigenvalue plot) gives the angular frequency, $\omega_k = \arctan(\mathrm{Im}\{\lambda_k\}/\mathrm{Re}\{\lambda_k\})$ with which the mode evolves in time. The absolute value, $|\lambda_k|$ represents the rate of growth ($|\lambda_k| > 1$) or decay ($|\lambda_k| < 1$) of the mode. The DMD eigenvalues correspond to the Strouhal number (St) and its harmonics. We order the DMD modes in increasing order of ω_k, neglecting the complex conjugates. Unless stated otherwise, the DMD modes correspond to DMD analysis via a truncated SVD, retaining 99% of the energy.

Figure 6 shows the three most relevant modes obtained via Fourier decomposition, POD, and DMD. The Fourier modes correspond to St ($k = 0.2$) and its harmonics ($k = 0.4$ and 0.8). The three POD modes

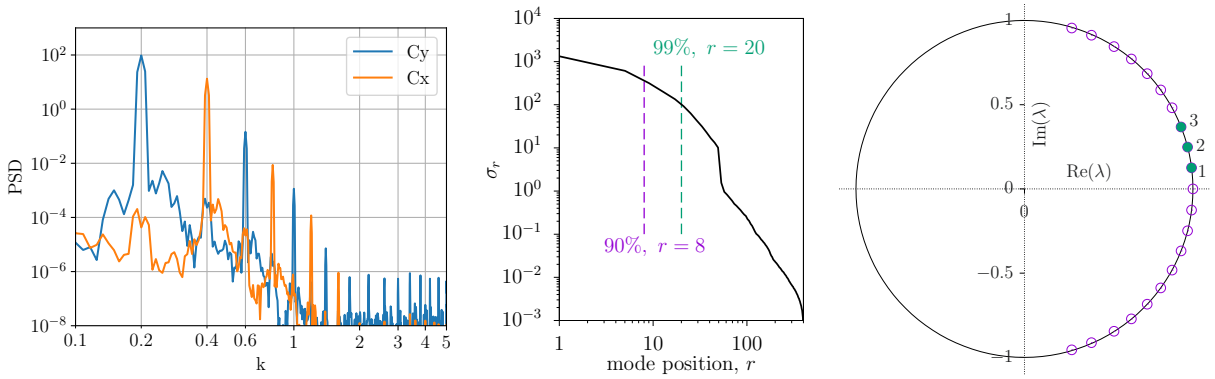

(a) PSDs of C_y and C_x (b) POD: σ (c) DMD: λ

Fig. 5: Results for $A/D = 0.25$: (a) power spectral densities (PSDs) of normal and tangential force coefficients (C_y and C_x), (b) singular values, σ from POD analysis, and (c) eigenvalues, λ from DMD.

correspond to the three largest singular values (σ). DMD modes are typically arranged according to the time dynamics given by their eigenvalues (λ). In the current analysis, the mode corresponding to the mean flow is ignored and the next three modes are plotted. These are identified in Fig. 5c using filled symbols and labeled using their mode number.

The three decomposition techniques give very similar dominant modes (Fig. 6). This result could be anticipated from the force spectra (Fig. 5a), which show that most of the system energy is contained in the vortex shedding frequency and its harmonics. Consequently, the Fourier modes are expected to correspond to the POD modes. The correspondence with DMD modes arises because the DMD eigenvalues align with the vortex shedding frequency and its harmonics. In Fig. 6, the odd-numbered modes (1 and 3) correspond to the vorticity that contributes to the normal force (C_y), making them topologically different from the even-numbered modes, which correspond to the tangential force (C_x). The 2S wake pattern is apparent in the odd-numbered modes but absent in the even-numbered modes.

3.2 P+S mode, $A/D = 0.5$

The P+S vortex pattern is observed in the cylinder wake for the $A/D = 0.5$ case (Fig. 4). This pattern is formed when one of the two shed vortices in an oscillation cycle splits into two vortices that convect downstream on either side of the cylinder. The other shed vortex, which does not split, pairs up with one of the split vortices. This pair of counter-rotating vortices is denoted as 'P'. The other part of the split vortex is denoted as 'S' for single vortex, and the combination of P and S is referred to as 'P+S'.

The spectra of the force coefficients (Fig. 7a) show a few more dominant harmonics and higher energy levels at high harmonics ($k > 1$) than observed for the $A/D = 0.25$ case. Due to the asymmetry in the vortex pattern, both odd and even-harmonics of St ($k = 0.2$) are observed in the C_y and C_x spectra The first 10 POD modes contain 90% of the energy (see Fig. 7b), making this case amenable to dimensional reduction.

Figure 8 compares the top three mode shapes obtained using the three modal decomposition strategies considered here. The P+S vortex structure is clearly visible in all these modes. Unlike the $A/D = 0.25$ case, the even-numbered modes are not topologically different from the odd-numbered modes. The mode shapes obtained with the three approaches are similar, for reasons discussed earlier - the highest energy modes are harmonics of St. The dominant DMD eigenvalues lie on the unit circle; however, those corresponding to higher harmonics of St have $|\lambda| < 1$, indicating the transient nature of these modes. However, these modes contain only a small fraction of the total energy.

3.3 2S mode, $A/D = 0.75$

The 2S vortex pattern reappears as the displacement oscillation amplitude is increased to $A/D = 0.75$. However, the dynamics in this case are richer than for $A/D = 0.25$. The general behavior expected of the

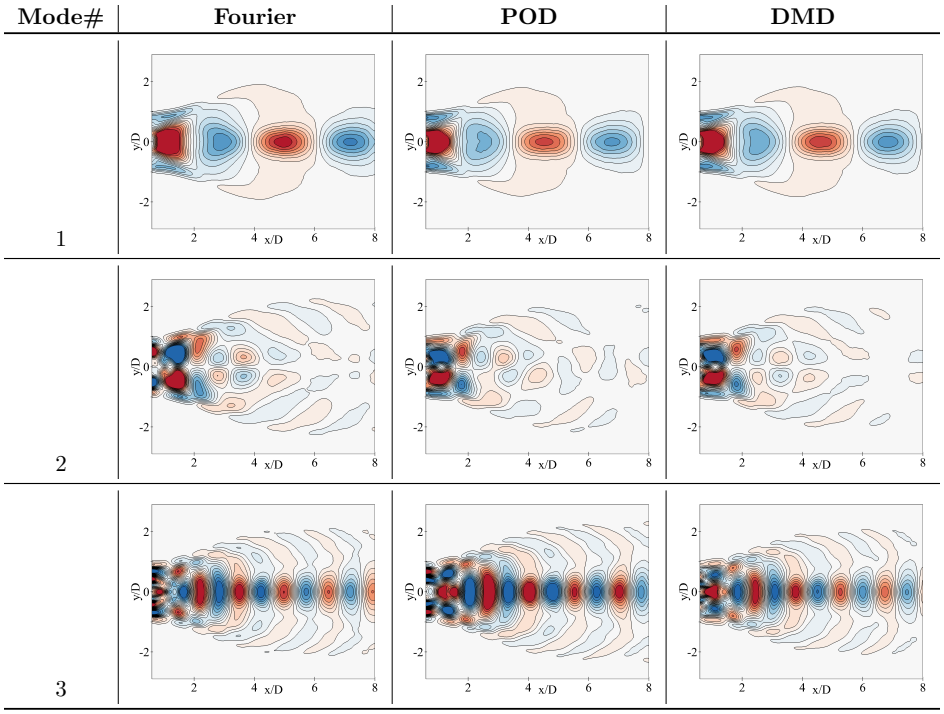

Fig. 6: Modal decomposition for $A/D = 0.25$; 2S mode

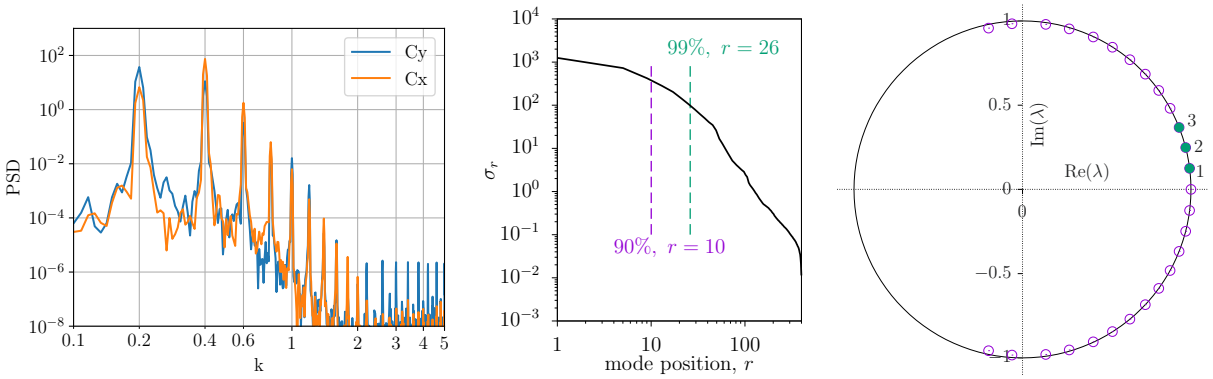

(a) PSDs of C_x and C_y (b) POD: σ (c) DMD: λ

Fig. 7: Results for $A/D = 0.5$: (a) power spectral densities (PSDs) of normal and tangential force coefficients (C_y and C_x), (b) singular values, σ from POD analysis, and (c) eigenvalues, λ from DMD.

2S wake pattern – odd harmonics of St in C_y and even harmonics in C_x spectra – is still observed (Fig. 9a). However, there is moderate energy in frequencies that are not harmonics of St.

The POD results show that while 90% of the variance can be captured with 13 modes, as many as 60 modes are required to represent 99% of the energy (Fig. 9b). Retaining 60 POD modes for the DMD analysis results in a crowded eigenvalue plot (Fig. 9c). Several DMD modes are present with λ in the region corresponding to the first three harmonics of St. The eigenvalue plot is significantly cleaner if 13 POD modes are retained, capturing 90% (as opposed to 99%) of the variance, for the DMD analysis (Fig. 10). The dominant DMD modes are equispaced on the unit circle and correspond to the Fourier modes that are harmonics of St. A heavily damped mode, corresponding to the complex conjugate pair of λ far inside the unit circle, is also observed.

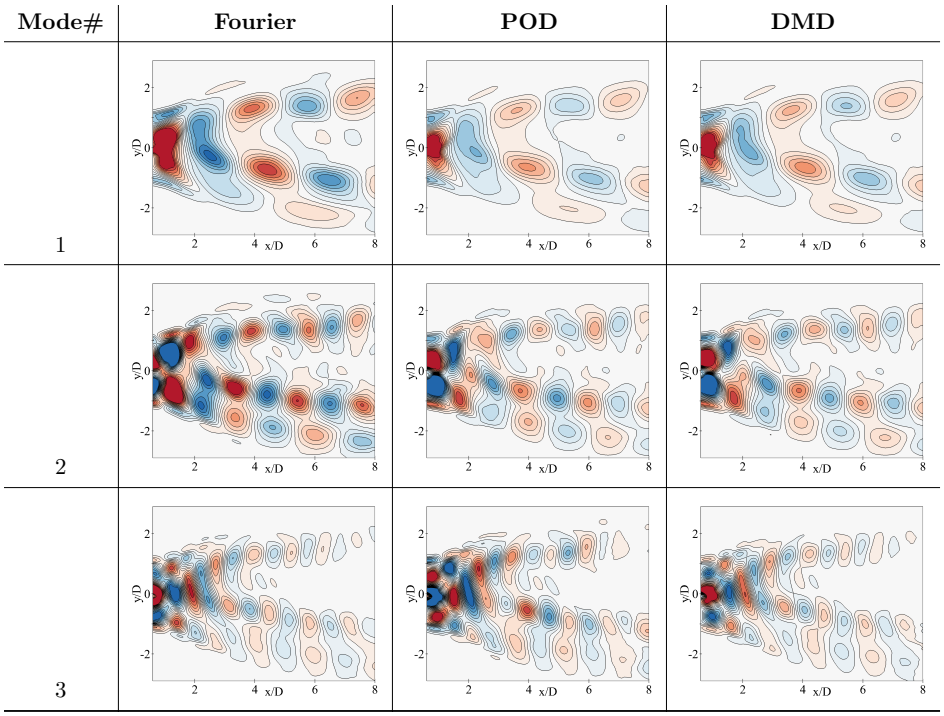

Fig. 8: Modal decomposition for $A/D = 0.5$; P+S mode

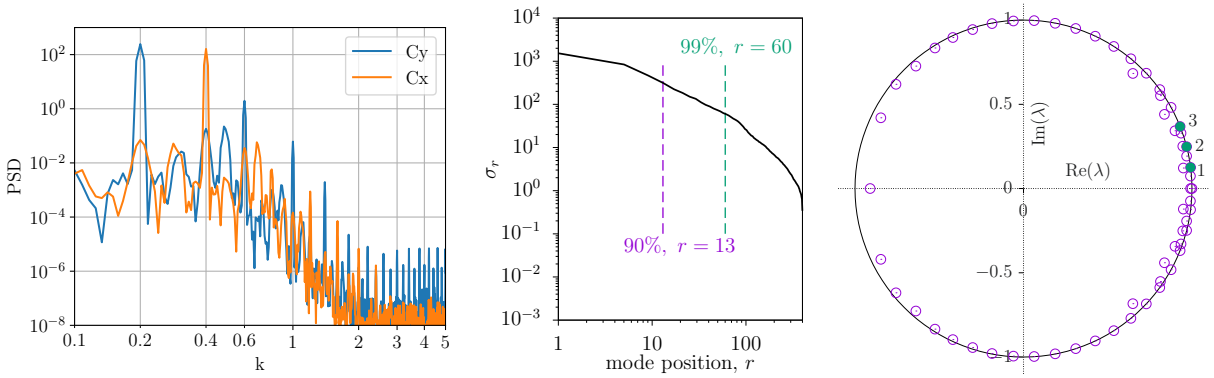

(a) PSDs of C_x and C_y (b) POD: σ (c) DMD: λ

Fig. 9: Results for $A/D = 0.75$: (a) power spectral densities (PSDs) of normal and tangential force coefficients (C_y and C_x), (b) singular values, σ from POD analysis, and (c) eigenvalues, λ from DMD.

Figure 11 shows that mode 1 from each decomposition technique is nearly the same and displays the 2S wake pattern. Mode 2 from Fourier analysis and DMD are similar, at least topologically, and resemble the mode 2 shape obtained for the $A/D = 0.25$ case. These modes represent the vorticity corresponding to the tangential force (C_x). The second mode from POD however, shows a 2S pattern and seems to match mode 3 of Fourier and DMD analysis. In fact, POD modes 2 and 3 seem to be swapped; this is confirmed by checking the time dynamics of these two POD modes (not shown), which show higher-frequency content in mode 2 than in mode 3. Note that POD modes are not associated with a single frequency or growth/decay rate. Since POD modes are organized based on variance, POD mode 2 has higher energy than mode 3. The spectra in Fig. 9a do not show the peak at $k = 0.6$ to be higher than the peak at $k = 0.4$. The higher energy in POD mode 3 is therefore likely due to features associated with other frequencies.

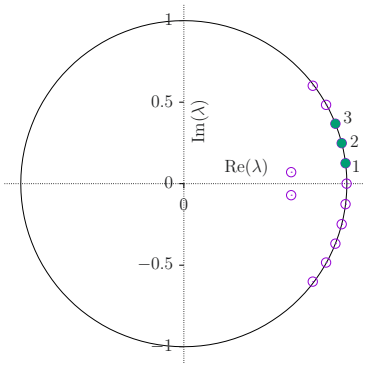

Fig. 10: DMD eigenvalues for $A/D = 0.75$ when a reduced number (=13) of POD modes representing 90% variance, are retained for the DMD analysis.

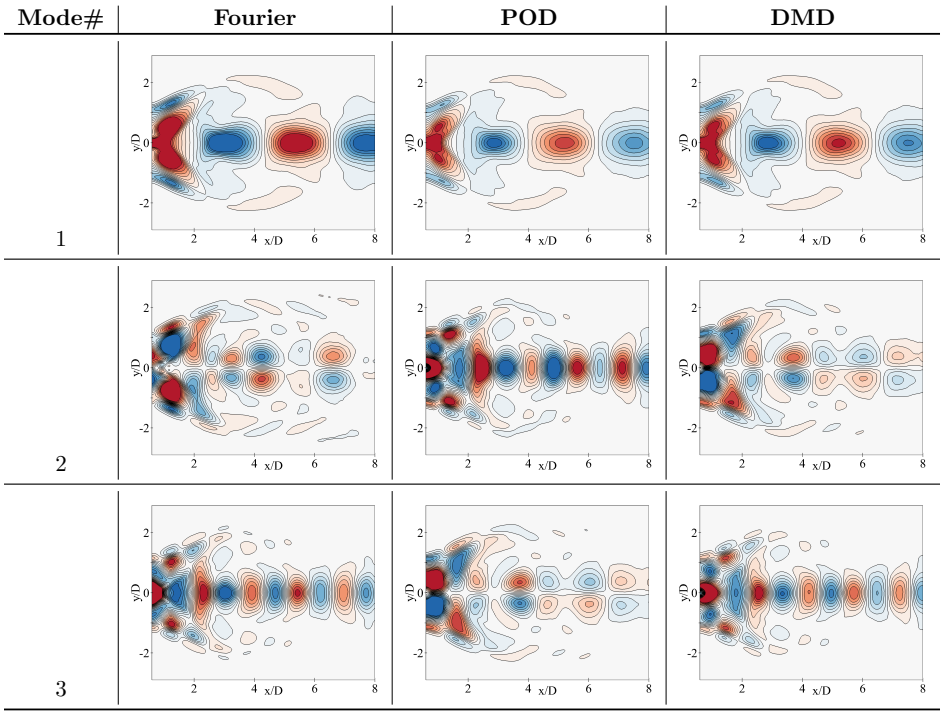

Fig. 11: Modal decomposition for $A/D = 0.75$; 2S mode. DMD mode shapes correspond to the analysis with a reduced ($r = 13$) number of POD modes retaining 90% of the energy.

3.4 2P mode, $A/D = 1.0$

The 2P vortex pattern is observed in the wake when A/D is increased to 1. Each of the two vortices shed from the cylinder during one cycle of oscillation splits into two vortices, forming a total of four vortices per cycle. These vortices convect downstream as two pairs (2P) of vortices of opposing signs, on either side of the cylinder making the wake symmetric. The spectra of the force coefficients look qualitatively similar to those in cases where the 2S wake pattern is observed – even harmonics of St contributing to C_x and odd harmonics contributing to C_y.

Despite the higher displacement amplitude, fewer POD modes (= 34) are required to capture 99% of the energy for this case compared to the $A/D = 0.75$ case, where 60 modes are needed. The DMD eigenvalue plot (Fig. 12c) is also cleaner, with the eigenvalues equispaced on the unit circle and corresponding to the

harmonics of St. We note that the amenability of dimensional reduction does not reduce monotonically with increasing oscillation amplitude.

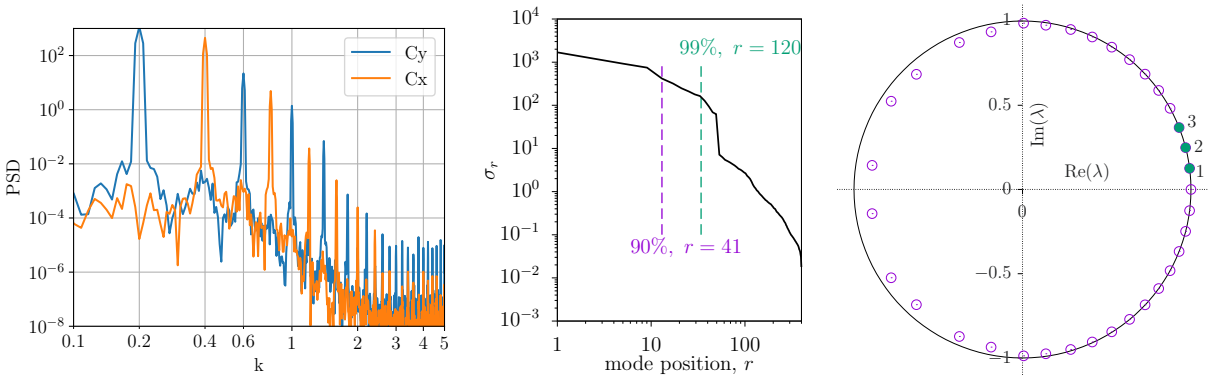

(a) PSDs of C_x and C_y (b) POD: σ (c) DMD: λ

Fig. 12: Results for $A/D = 1.0$: (a) power spectral densities (PSDs) of normal and tangential force coefficients (C_y and C_x), (b) singular values, σ from POD analysis, and (c) eigenvalues, λ from DMD.

The mode shapes predicted by Fourier analysis, POD, and DMD agree very well for modes 1 and 2. Differences can be observed between the POD mode and the Fourier and DMD modes for mode 3. A higher cross-stream wavenumber is observed for the Fourier and DMD modes, whereas the POD mode shape retains the vortex structure in the cross-stream direction.

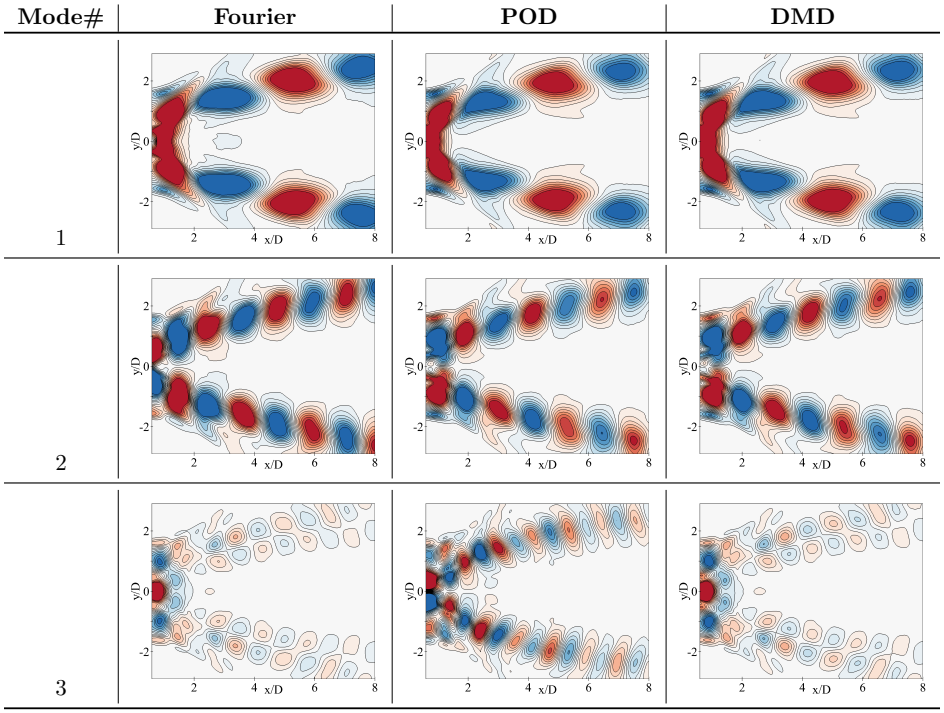

Fig. 13: Modal decomposition for $A/D = 1.0$; 2P mode

3.5 Combination mode, $A/D = 0.9$

For $A/D = 0.9$, the wake vorticity patterns continually shift between 2P and 2S in time. The force spectra show higher broadband levels than in the other cases (Fig. 14a). Only the peaks at $k = 0.2$ and 0.4 are prominent (two or more orders of magnitude above the broadband level); the other peaks are not distinguishable. The POD analysis shows that a large number of modes (= 41) are required to represent 90% of the system's energy (Fig. 14b). The eigenvalue plot in Fig. 14c shows that the DMD modes are continuously distributed over a wide frequency range, not just at multiples of St. Additionally, multiple modes, including some that show exponential decay ($\lambda < 1$), crowd the region around the first five harmonics of St.

Figure 15 compares the mode shapes for this case. The switch between the 2P and 2S wake patterns occurs every 1.5 cycles of cylinder oscillation. At this frequency of switching, both wake patterns are simultaneously present in the window used for performing modal decomposition. As a consequence, these wake patterns are not identified as *distinct* modes by any of the three decomposition techniques.

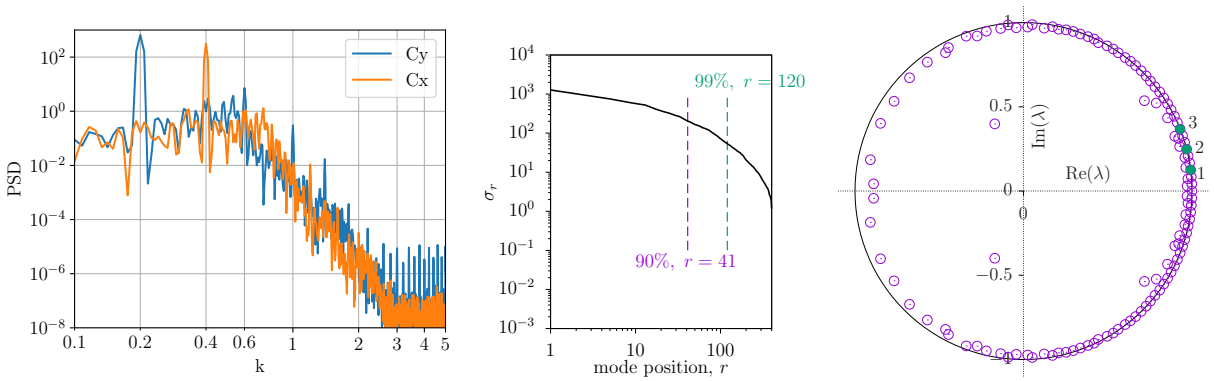

(a) PSDs of C_x and C_y (b) POD: σ (c) DMD: λ

Fig. 14: Results for $A/D = 0.9$: (a) power spectral densities (PSDs) of normal and tangential force coefficients (C_y and C_x), (b) singular values, σ from POD analysis, and (c) eigenvalues, λ from DMD.

The wake vorticity continually shifts between the 2P and 2S modes for the $A/D = 0.9$ case. This is a part of a gradual progression from 2S to 2P as the cylinder oscillation amplitude increases from $A/D = 0.7$ to 1.0. At $A/D = 0.8$, a 2P/2S shifting is observed, with 2P and 2S appearing alternately every cycle of cylinder oscillation. At $A/D = 0.9$, a similar switching occurs, but in this case, the pattern shifting is less frequent, with the 2P pattern lasting longer than the 2S pattern in every cycle. We investigate mrDMD modes for $A/D = 0.9$ at $k = 0.2$ and $k = 0.4$, for which the force spectra (Fig. 14a) show prominent peaks.

Figure 16 illustrates the mrDMD process. We consider 400 snapshots in time and the spatial grid is 600×400. Five resolutions/levels are selected and the frequency ranges retained are $0.025 - 0.035$ (in the lowest level) and $0.40 - 0.56$ (in the highest level). Slow-mode cutoff is given by $\rho_l = \text{max\_cyc}\ /T_l$ with $\text{max\_cyc} = 5 - 7$, retaining modes with $\leq$ 5-7 cycles per window. These parameters provide good time localization of intermittent and transient dynamics, with bin lengths decreasing from 200 at level 1 to ~ 12.5 (~ 25 snapshots) at level 5, corresponding to the stated frequency cutoffs. For $k = 0.2$, represented by Level 3 in the figure, the time window over which data is collected, is divided into four time bins. The slowest mrDMD modes corresponding to each of the time bins are plotted in Fig. 17, which does not show switching between 2P and 2S.

For $k = 0.4$, represented by Level 4 in Fig. 16, the entire time window is divided into eight bins. The dominant mrDMD modes corresponding to the first six time bins are plotted in Fig. 18, where the switching between the 2P and 2S modes is clearly visible. The first time bin exhibits a 2P mode, the second bin shows a distorted 2P mode (indicating mode transition), and the third bin displays a 2S mode. This pattern repeats in time bins 4 through 6, as shown in Fig. 18. The switching between the 2P and 2S modes, which occurs with a period of 37.5 time units (equivalent to 1.5 cycles of cylinder oscillation), is thus captured at the $k = 0.4$ level in the mrDMD analysis.

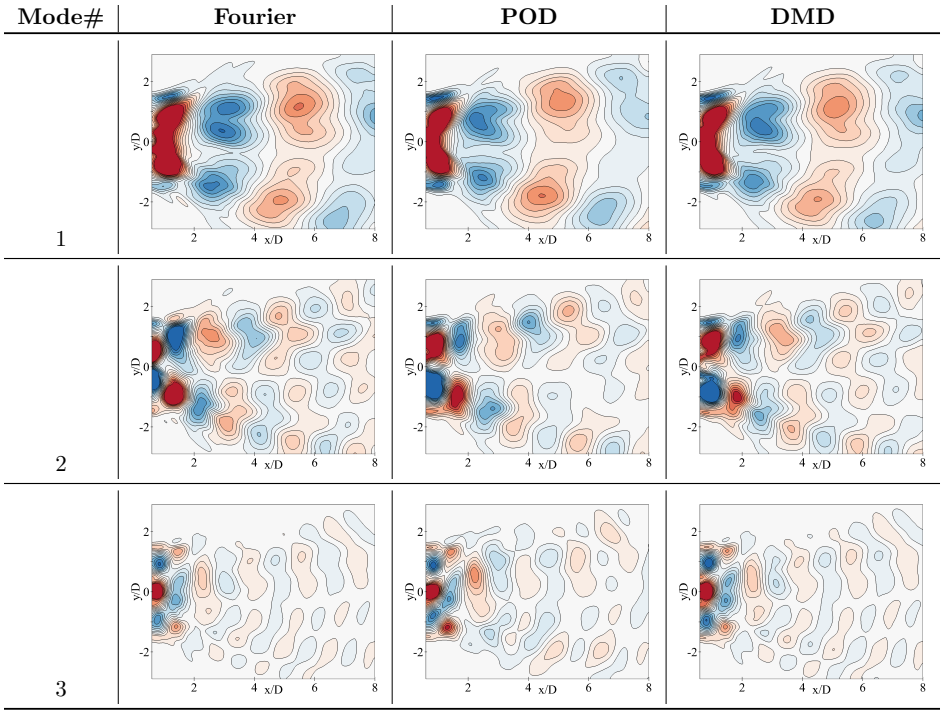

Fig. 15: Modal decomposition for $A/D = 0.9$; combination mode. DMD mode shapes correspond to the analysis with a reduced ($r = 41$) number of POD modes retaining 90% of the energy.

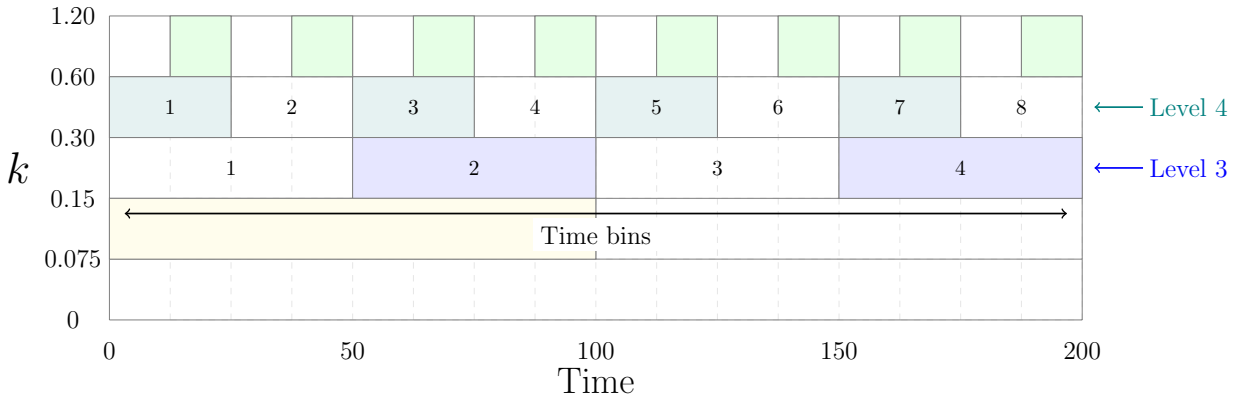

Fig. 16: Time-frequency decomposition (mrDMD) for $A/D = 0.9$; cylinder oscillation period is 25 time units.

Note that the dynamics of the 2S and 2P modes are the same, hence these modes are not separated into different k levels (Fig. 16). However, they are separated in time. Hence, when the size of the time bin for mrDMD analysis corresponds to the time period of the 2P/2S modes, then they can be separated out, as seen in Fig. 18. At Level 4, where each time bin corresponds to 25 time units, the mrDMD mode extracted is either a 2P mode, a 2S mode, or a mode transitioning between 2P and 2S. Similar results are obtained for the $A/D = 0.8$ case (see Section B).

3.6 Windowed Fourier Transform, POD, and DMD

As noted in the mrDMD analysis, modal transitions are separated only in time, not in frequency. Therefore, the property of mrDMD that is critical for mode identification here is 'windowing' in time. This observation

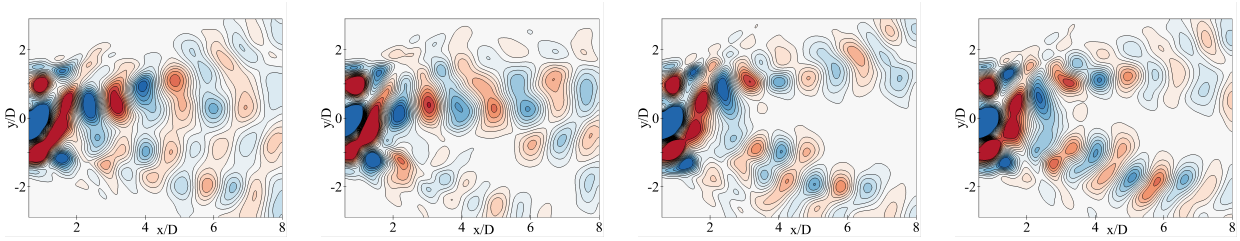

(a) bin 1 (b) bin 2 (c) bin 3 (d) bin 4

Fig. 17: Level 3 mrDMD modes for $A/D = 0.9, k = 0.2$; 2S/2P mode switching is not observed at this frequency level.

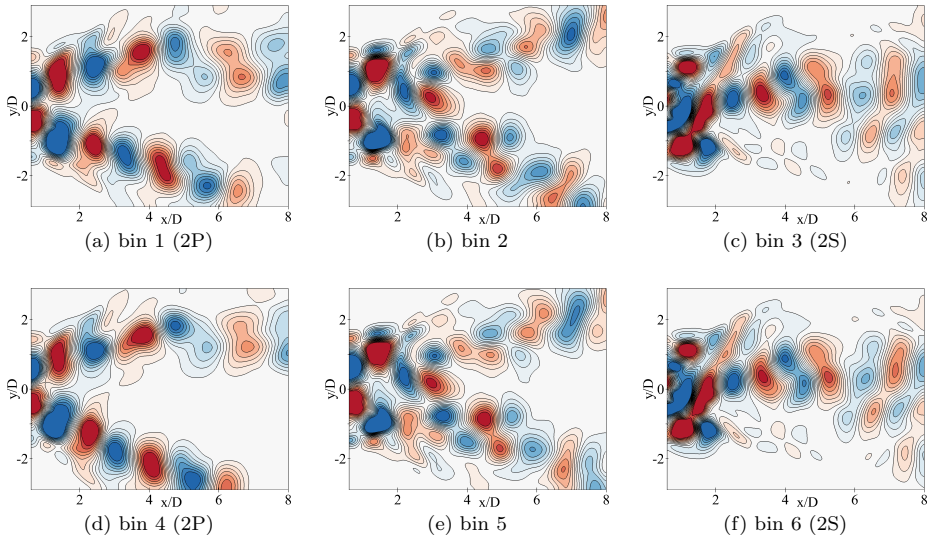

(a) bin 1 (2P) (b) bin 2 (c) bin 3 (2S)

(d) bin 4 (2P) (e) bin 5 (f) bin 6 (2S)

Fig. 18: Level 4 - mrDMD decomposition for $A/D = 0.9$. Mode switching (between 2P and 2S) occurs every 1.5 cycles of cylinder oscillation; each time bin (25 time units) is equal to the cylinder oscillation period.

suggests that the modal decomposition methods such as the Fourier transform (FT), POD, and DMD should also be effective if applied on appropriately sized time windows of data. To verify this hypothesis, we perform windowed FT, POD, and DMD, selecting a time window of 25 time units (corresponding to the mode transition period of 1.5 cycles of cylinder oscillation for the $A/D = 0.9$ case) and translating the window across the time horizon. Figure 23 shows the results for the windowed DMD analysis. As hypothesized, the 2P, 2S, and 2P/2S modes are as clearly visible in the windowed DMD results as in the mrDMD results (compare Figs. 18 and 19). A similar delineation is achieved with windowed POD and DFT analyses (see Section C).

4 Conclusions

Four modal decomposition techniques—Fourier analysis, proper orthogonal decomposition (POD), dynamic mode decomposition (DMD), and multiresolution DMD (mrDMD)—are used to analyze the wake structure of a transversely oscillating cylinder in flow at a diameter-based Reynolds number of 500. The cylinder is prescribed to move sinusoidally at a frequency equal to the vortex shedding frequency of a static cylinder. Multiple cases are analyzed, with the scaled displacement amplitude (A/D) varying between 0.2 and 1.0.

While the system is generally linear for small A/D, the amenability of dimensional reduction does not decrease monotonically with increasing A/D. For example, the case with $A/D = 1.0$ requires fewer POD modes to represent 99% of the signal energy compared to cases with $A/D = 0.75$, 0.8, and 0.9. Additionally, the mode shapes for $A/D = 1.0$ correspond to the harmonics of the Strouhal number.

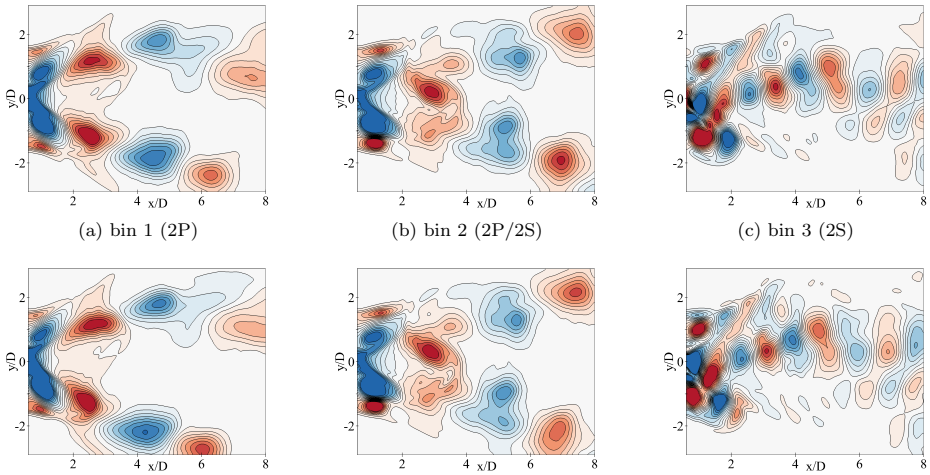

(a) bin 1 (2P) (b) bin 2 (2P/2S) (c) bin 3 (2S)

(d) bin 4 (2P) (e) bin 5 (2P/2S) (f) bin 6 (2S)

Fig. 19: Windowed DMD for $A/D = 0.9$; 2P/2S combination mode

Dimensional reduction is readily achievable in cases where the force spectra exhibit dominant peaks. In such cases, the dominant modes obtained from Fourier analysis, POD, and DMD are very similar. DMD and Fourier modes are found to be closer to each other than to POD modes, though the differences are small. For these cases, mrDMD does not provide any additional information.

Intermittency (mode switching) is observed for $A/D = 0.8$ and 0.9, with the 2P and 2S modes appearing alternately in the wake. Since mode switching occurs over time, mrDMD effectively isolates these modes by leveraging its hierarchical time-series subdivision. In contrast, DMD, POD, and DFT, which are typically applied to the entire time series without predefined temporal segmentation, struggle to capture these transitions. However, when applied over appropriate time windows, these methods perform just as effectively as mrDMD in delineating the intermittent modes and patterns.

Acknowledgments

Funding for this research is provided by the National Science Foundation (CMMI-1537917, CBET-1554196 and 1935255). We also acknowledge the computational resources provided by the US Department of Defense (AFOSR Award# FA9550-23-1-0016) and Iowa State University.

Data availability statement

The data that support the findings of this study are available from the corresponding author upon reasonable request.

References

Bagheri, S.: Koopman-mode decomposition of the cylinder wake. Journal of Fluid Mechanics **726**, 596–623 (2013)

Berkooz, G., Holmes, P., Lumley, J.L.: The proper orthogonal decomposition in the analysis of turbulent flows. Annual Review of Fluid Mechanics **25**(1), 539–575 (1993)

Govardhan, R., Williamson, C.: Modes of vortex formation and frequency response of a freely vibrating cylinder. Journal of Fluid Mechanics **420**, 85–130 (2000)

Huera-Huarte, F.J., Vernet, A.: Vortex modes in the wake of an oscillating long flexible cylinder combining pod and fuzzy clustering. Experiments in fluids **48**(6), 999–1013 (2010)

Kutz, J.N., Brunton, S.L., Brunton, B.W., Proctor, J.L.: Dynamic Mode Decomposition: Data-driven Modeling of Complex Systems. Society for Industrial and Applied Mathematics, ??? (2016)

Kutz, J.N., Fu, X., Brunton, S.L.: Multiresolution dynamic mode decomposition. SIAM Journal on Applied Dynamical Systems **15**(2), 713–735 (2016)

Khalak, A., Williamson, C.: Fluid forces and dynamics of a hydroelastic structure with very low mass and damping. Journal of Fluids and Structures **11**(8), 973–982 (1997)

Kou, J., Zhang, W., Liu, Y., Li, X.: The lowest reynolds number of vortex-induced vibrations. Physics of Fluids **29**(4), 041701 (2017)

Leontini, J.S., Stewart, B.E., Thompson, M.C., Hourigan, K.: Wake state and energy transitions of an oscillating cylinder at low reynolds number. Physics of fluids **18**(6), 067101 (2006)

Lumley, J.L.: The structure of inhomogeneous turbulent flows. Atmospheric turbulence and radio wave propagation (1967)

Morse, T., Williamson, C.: Employing controlled vibrations to predict fluid forces on a cylinder undergoing vortex-induced vibration. Journal of Fluids and Structures **22**(6-7), 877–884 (2006)

Morse, T., Williamson, C.: Prediction of vortex-induced vibration response by employing controlled motion. Journal of Fluid Mechanics **634**, 5 (2009)

Sarpkaya, T.: A critical review of the intrinsic nature of vortex-induced vibrations. Journal of Fluids and Structures **19**(4), 389–447 (2004)

Schmid, P.J.: Dynamic mode decomposition of numerical and experimental data. Journal of Fluid Mechanics **656**, 5–28 (2010)

Tissot, G., Cordier, L., Benard, N., Noack, B.R.: Dynamic mode decomposition of PIV measurements for cylinder wake flow in turbulent regime. In: Eighth International Symposium on Turbulence and Shear Flow Phenomena (2013). Begel House Inc.

Vandiver, J.K.: Damping parameters for flow-induced vibration. Journal of Fluids and Structures **35**, 105–119 (2012)

Welch, P.: The use of fast fourier transform for the estimation of power spectra: a method based on time averaging over short, modified periodograms. IEEE Transactions on audio and electroacoustics **15**(2), 70–73 (1967)

Wu, X., Jafari, M., Sarkar, P., Sharma, A.: Verification of DES for flow over rigidly and elastically-mounted circular cylinders in normal and yawed flow. Journal of Fluids and Structures **94**(102895) (2020)

Wang, S., Liu, Y.Z.: Flow structures behind a vibrissa-shaped cylinder at different angles of attack: Complication on vortex-induced vibration. International Journal of Heat and Fluid Flow **68**, 31–52 (2017)

Williamson, C.H., Roshko, A.: Vortex formation in the wake of an oscillating cylinder. Journal of fluids and structures **2**(4), 355–381 (1988)

Wu, X., Sharma, A.: Artefacts of finite span in vortex-induced vibration simulations. Applied Ocean Research **101**, 102265 (2020)

Wu, X., Sharma, A., Jafari, M., Sarkar, P.: Towards predicting dry cable galloping using detached eddy simulations. In: 55th AIAA Aerospace Sciences Meeting, p. 1483 (2017)

Wu, X.: Numerical investigation of flow over elastically-mounted circular cylinders. PhD thesis, Iowa State

University (2020)

Appendices

A Mode decomposition in a frame moving with the cylinder

The numerical results are natively available in a frame of reference attached to the cylinder since the computational mesh moves with the cylinder. However, wake vorticity patterns in the literature have been primarily reported and analyzed in the ground frame of reference since a) such patterns are obtained from flow visualization which is easier to perform in the ground frame, and b) the cylinder frame is non-inertial, which convolutes the results and makes interpreting them difficult. The CFD solution in the cylinder wake region is therefore interpolated onto a mesh that is stationary in the ground frame to obtain the results presented in the main paper.

In this appendix, we compare modal decomposition results obtained using data in the cylinder frame of reference with those obtained using data in the ground frame of reference. Only the DMD modes are compared and the comparison is limited to two displacement amplitudes: $A/D = 0.25$ and 1.0, which represent small and large oscillation amplitudes respectively. Figure 20 compares the results. At small A/D, the differences between the DMD modes in the ground frame and the cylinder frame are small. At high A/D however, the non-inertial effects overwhelm the results and the mode shapes in the cylinder frame show no resemblance to those in the ground frame. This observations also applies to Fourier analysis, POD, and mrDMD.

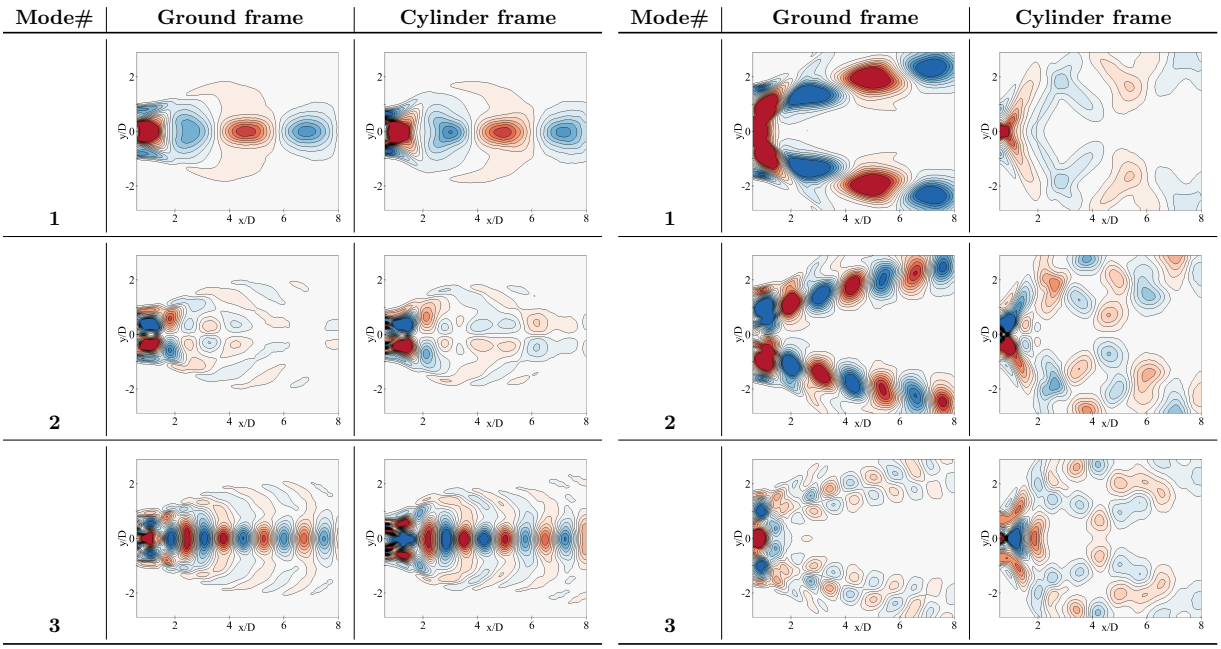

(a) $A/D = 0.25$ (b) $A/D = 1.0$

Fig. 20: Comparison of DMD modes in the ground and cylinder frames of reference for two cases.

B mrDMD results for $A/D = 0.8$

Multi-resolution DMD results for $A/D = 0.8$ are similar to those for $A/D = 0.9$, except the switching between the 2S and 2P modes is faster—occurring every cycle of cylinder oscillation. Figure 21 shows the first six mrDMD modes for time-level 4 (see Fig. 16). For mrDMD modes corresponding to $k = 0.4$, each time bin (equal to the cylinder oscillation period) shows the 2P and 2S modes appearing alternately. Similar to the $A/D = 0.9$ case, mode switching is not discernible for frequency level 3, which corresponds to $k = 0.2$.

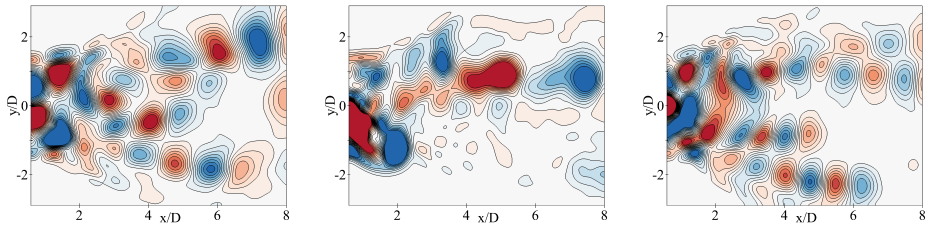

(a) bin 1 (2P) (b) bin 2 (2S) (c) bin 3 (2P)

(d) bin 4 (2S) (e) bin 5 (2P) (f) bin 6 (2S)

Fig. 21: Level 4 - mrDMD decomposition for $A/D = 0.8$; 2P and 2S modes appears alternately in every time bin. For this time level, a time bin (25 units) is equal to cylinder oscillation period.

C Windowed POD and Fourier analysis for $A/D = 0.9$

Windowed POD analysis for $A/D = 0.9$ reveals the switching between 2S and 2P modes. Figure 22 presents the most dominant POD mode for the first six time bins. While these modes differ slightly from those obtained using mrDMD and windowed DMD, they nonetheless capture the transition between 2P and 2S mode patterns.

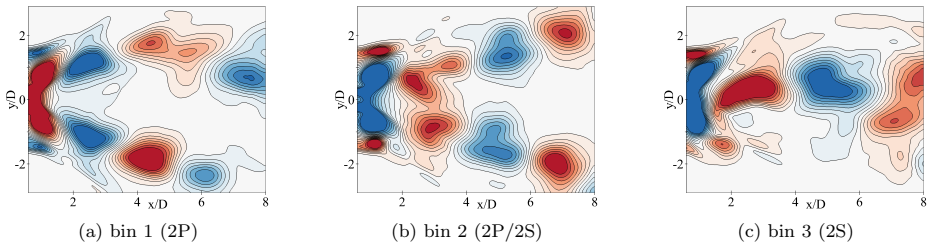

(a) bin 1 (2P) (b) bin 2 (2P/2S) (c) bin 3 (2S)

(d) bin 4 (2P) (e) bin 5 (2P/2S) (f) bin 6 (2S)

Fig. 22: Windowed POD for $A/D = 0.9$; 2P/2S combination mode

Figure 23 illustrates the dominant Fourier modes corresponding to the first six time bins for $k = 0.2$ and 0.4. These frequency components coincide with the peaks observed in the force spectra for $A/D = 0.9$. Notably, the Fourier modes within these time windows exhibit similarities to those identified using mrDMD, and windowed DMD and POD, capturing the expected transition from 2P to 2S modes.

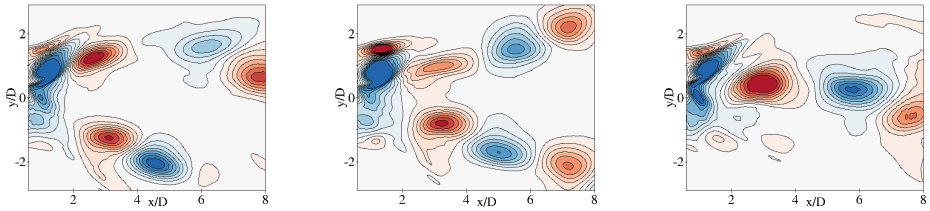

(a) bin 1 (2P) (b) bin 2 (2P/2S) (c) bin 3 (2S)

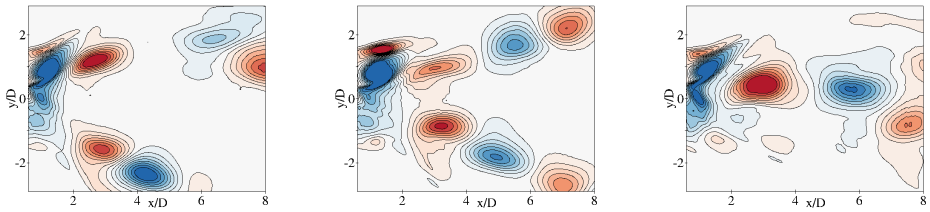

(d) bin 4 (2P) (e) bin 5 (2P/2S) (f) bin 6 (2S)

(a) $k = 0.2$

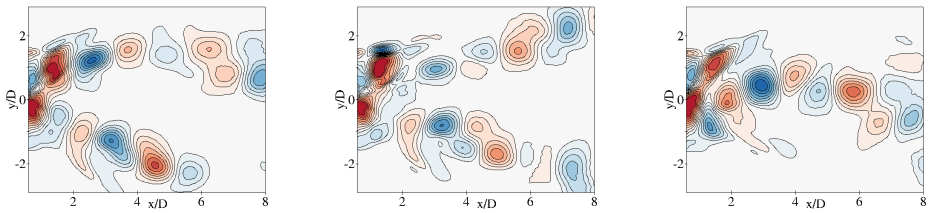

(a) bin 1 (2P) (b) bin 2 (2P/2S) (c) bin 3 (2S)

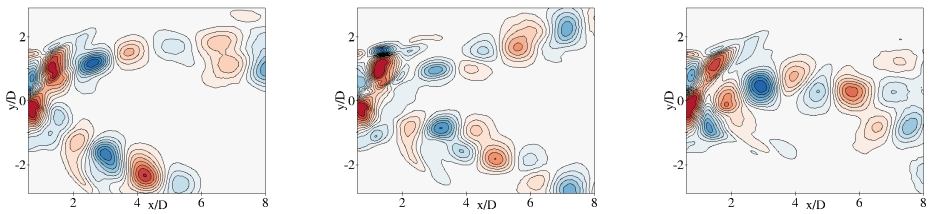

(d) bin 4 (2P) (e) bin 5 (2P/2S) (f) bin 6 (2S)

(b) $k = 0.4$

Fig. 23: Windowed fourier analysis for $A/D = 0.9$ for two values of k.